Flux-Weakening Strategy of an Induction Machine Driven by an Electrolytic-Capacitor-Less Inverter

Anno Yoo, *Member, IEEE*, Seung-Ki Sul, *Fellow, IEEE*, Hyeseung Kim, and Kyung-Seo Kim, *Member, IEEE*

***Abstract*—This paper presents a novel flux-weakening strategy for an induction machine driven by an electrolytic-capacitor-less inverter. In the electrolytic-capacitor-less inverter, the dc-link voltage is fluctuating at six times the frequency of the input three-phase source due to its small dc-link capacitance. Hence, the decoupling of the fluctuation and maximum utilization of the dc-link voltage is a major issue in the electrolytic-capacitor-less inverter. In this paper, the cost function is set to increase the voltage utilization of the inverter for the flux-weakening operation of an induction machine. With the proposed flux-weakening strategy, the operating speed of the induction machine is extended above the base speed without any stability problems. The experimental results show the effectiveness of the proposed strategy.**

***Index Terms*—Electrolytic-capacitor-less inverter, flux-weakening operation, induction machine.**

I. Introduction

RECENTLY, the size and cost of reactive components such as inductors and electrolytic capacitors have become main concerns in the design of dc-link-based ac–dc–ac power converters. In particular, the large electrolytic capacitors in the dc link are bulky and expensive [1]. Moreover, the life expectancy of electrolytic capacitors is typically shorter than any of the other components in the converters, and an additional precharging circuit is necessary to reduce the inrush current to the large capacitor bank. Although the precharging time is very short compared to the total operation periods, the cost and volume of the circuit are not negligible.

For these reasons, many studies have attempted to reduce the dc-link capacitance [2]–[7]. With the reduced dc-link capacitor, the total harmonic distortion (THD) of the input phase current can be improved remarkably, and the total volume and the cost can be reduced.

There are several types of reduced-dc-link-capacitance voltage-source inverter (VSI). The converter proposed in [3] uses a diode front-end (DFE) rectifier and a reduced dc-link capacitor. By using a DFE rectifier, the inverter can operate only in the motoring mode, and its application is restricted such as a fan or a pump. In several studies [4], [5], an active front-end (AFE) rectifier identical to a pulsewidth modulation (PWM) boost converter with a reduced dc-link capacitor was introduced. Although its input phase current is nearly sinusoidal and a bidirectional power flow is possible due to the AFE rectifier, installation of large interface inductors between the grid and the AFE rectifier is required. These large interface inductors can increase the volume and the cost. Moreover, the size of the dc-link capacitor is dependent on the load power. That is, higher load power demands a larger dc-link capacitor. In another study [6], a PWM boost converter using a small dc-link capacitor was demonstrated. However, its performance was sensitive to variations in the parameters. An electrolytic-capacitor-less inverter with a bidirectional rectifier has also been presented [2], [13]. Although installation of an input filter is necessary on the grid side, the inductance of the input filter is quite small compared to the interface inductors of an AFE rectifier; moreover, this power converter can be operated in both motoring and regenerating modes due to its bidirectional rectifier. With these advantages, it can be incorporated with the proposed flux-weakening algorithm in this paper.

However, in the research mentioned earlier, the main focus has been on the constant-torque region operation of the induction machine. It is also important to determine how to synthesize the output voltage of the PWM inverter not only in the constant-torque region but also in the flux-weakening region because the dc-link voltage of the electrolytic-capacitor-less inverter is fluctuating according to the input voltage [13].

There had been several preferred approaches that enhance the flux-weakening performance of an induction machine. In [7], a simple flux-weakening operation using an electrolytic-capacitor-less inverter with a DFE rectifier was proposed. In this method, however, the maximum steady-state output voltage is limited to the minimum dc-link voltage, and the voltage available to the induction machine is restricted within the linear modulation region. In [8], the maximum torque control strategy of an induction machine in the flux-weakening region was addressed. However, this method depends on the machine parameters and does not consider variation of the dc-link voltage. Hence, its performance is limited and may degrade over all operating conditions, particularly in the case of an electrolytic-capacitor-less inverter. In [9], the rotor flux reference varies according to the speed, which is a commonly used method for the flux weakening of an induction machine. However, this method cannot obtain the maximum torque, as mentioned in [8]. Also, if the dc-link voltage is fluctuating, the base speed and the rotor flux reference should vary according to the dc-link

Manuscript received August 31, 2010; revised November 12, 2010; accepted December 4, 2010. Date of publication March 10, 2011; date of current version May 18, 2011. Paper 2010-IDC-356.R1, presented at the 2009 IEEE Energy Conversion Congress and Exposition, San Jose, CA, September 20–24, and approved for publication in the IEEE TRANSACTIONS ON INDUSTRY APPLICATIONS by the Industrial Drives Committee of the IEEE Industry Applications Society.

A. Yoo, H. Kim, and K.-S. Kim are with LSIS, Anyang 431-848, Korea (e-mail: realanno@eepel.snu.ac.kr; sjkim3@lsis.biz; kyungseok@lsis.biz).

S.-K. Sul is with Seoul National University, Seoul 151-742, Korea (e-mail: sulsk@plaza.snu.ac.kr).

Color versions of one or more of the figures in this paper are available online at http://ieeexplore.ieee.org.

Digital Object Identifier 10.1109/TIA.2011.2125936

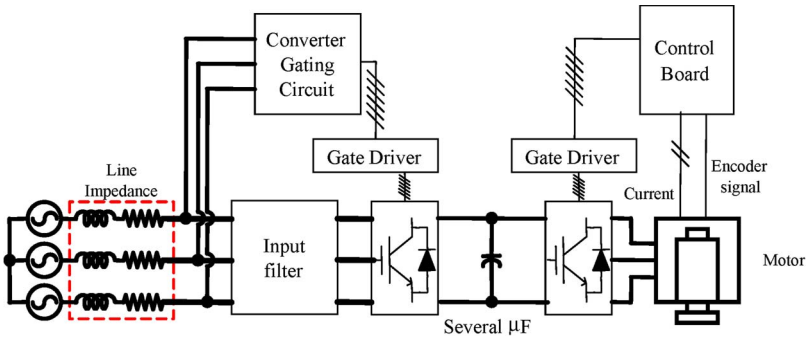

Fig. 1. Block diagram of the electrolytic-capacitor-less inverter.

voltage. In [10], a voltage control strategy is introduced for the flux-weakening operation of an induction machine. However, it is difficult to design the voltage controller when the dc-link voltage is fluctuating.

In this paper, a novel strategy for the flux-weakening operation of an induction machine is presented, which is driven by an electrolytic-capacitor-less inverter, as presented in [2] and [13]. The proposed flux-weakening strategy increases the voltage utilization under the continuous fluctuation of the dc-link voltage due to the small capacitance in the dc link. Based on the cost function, the dc-link voltage can be utilized maximally in the flux-weakening operation region. The experimental results show the effectiveness of the proposed flux-weakening method.

II. Analysis of an Electrolytic-Capacitor-Less Inverter With a Bidirectional Rectifier

Fig. 1 shows a block diagram of the electrolytic-capacitor-less inverter addressed in this paper. As shown in Fig. 1, there is only a film capacitor of several microfarads at the dc link in the case of a drive system of several kilowatts with a 380-$V_{\rm rms}$ ac three-phase input source. That is, there is no inductor and braking chopper in the dc link. However, an input filter is required to smooth the input current in the electrolytic-capacitor-less inverter because most of the PWM switching ripples of the inverter currents transfer to the input source due to small capacitance in the dc link. Considering the cost and the volume, an LC or an LCL filter with a damping resistor can serve as an input filter. In this paper, a simple LC filter with a damping resistor is used as the input filter.

Fig. 2 shows the experimental results of the input current and its frequency spectrum at 4-kW motoring mode at a line-to-line input voltage of 380 $V_{\rm rms}$. With the small dc-link capacitance, the input "a" phase current is a quasi-square wave, as shown in Fig. 2(a). In addition, the fifth and seventh harmonic currents are below 15% of the fundamental component, as shown in Fig. 2(b).

The dc-link voltage also undergoes inevitable fluctuation, whose frequency is six times the line frequency due to the small dc-link capacitance. The maximum and minimum values of the dc-link voltage are determined by the input line-to-line voltages as expressed by (1) and (2), respectively,

$$V_{\rm dc\_max} = \max\left(\sqrt{2}v_{\rm line-to-line}\right) \tag{1}$$

$$V_{\rm dc\_min} = \max\left(\sqrt{2}v_{\rm line-to-line}\right)\cos\left(\frac{\pi}{6}\right) \tag{2}$$

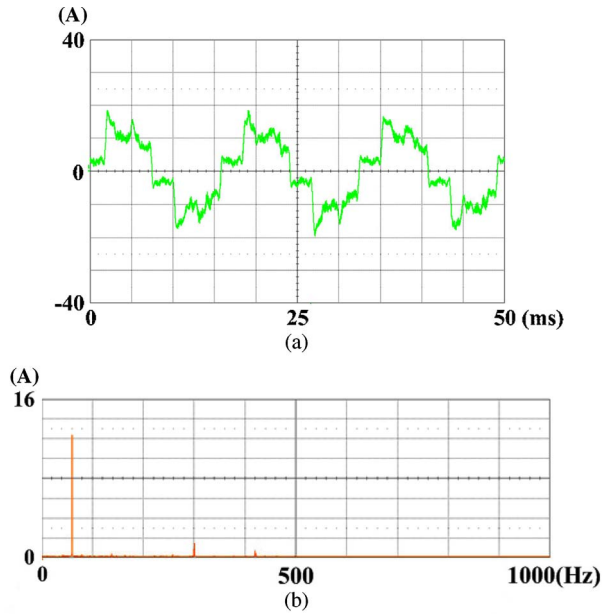

Fig. 2. Input current and fast Fourier transform (FFT) of the input current at 4-kW motoring mode. (a) Input "a" phase current. (b) FFT of the input current.

where $v_{\rm line-to-line}$ is the input line-to-line voltage in rms, $V_{\rm dc\_max}$ is the maximum dc-link voltage, and $V_{\rm dc\_min}$ is the minimum dc-link voltage.

As shown in (1) and (2), the minimum dc-link voltage is 86.6% of the maximum value theoretically. However, the dc-link voltage can vary according to the operation mode due to the effect of the input filter [13]. In particular, the minimum dc-link voltage at the motoring mode is much lower than that at the regenerating mode. Hence, it is important to determine how to synthesize the output voltage of the inverter under these fluctuating dc-link voltages.

Fig. 3 shows that the switching frequency of the bidirectional rectifier is identical to the frequency of the input line voltage. Although the structure is similar to that of the PWM boost converter, the switching instance of the converter is synchronized via parallel diode commutation. In addition, the operation of the bidirectional rectifier is not related to the operation of the PWM inverter part. The switching loss of the rectifier is also negligible compared to that of the PWM boost converter. In Fig. 3, the switching instants of the converter according to the line-to-line input voltage are shown. Due to the negligible switching

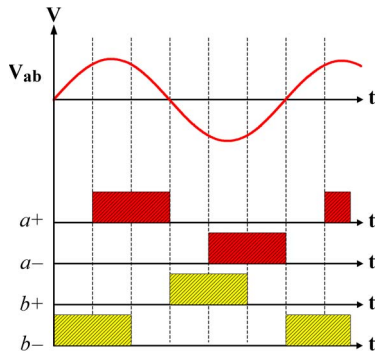

Fig. 3. Switching sequence of the bidirectional rectifier according to the input line-to-line voltage (V_{ab}: "ab" line-to-line voltage, $a+$: "a" phase upper switch, $a-$: "a" phase lower switch, $b+$: "b" phase upper switch, $b-$: "b" phase lower switch of the rectifier).

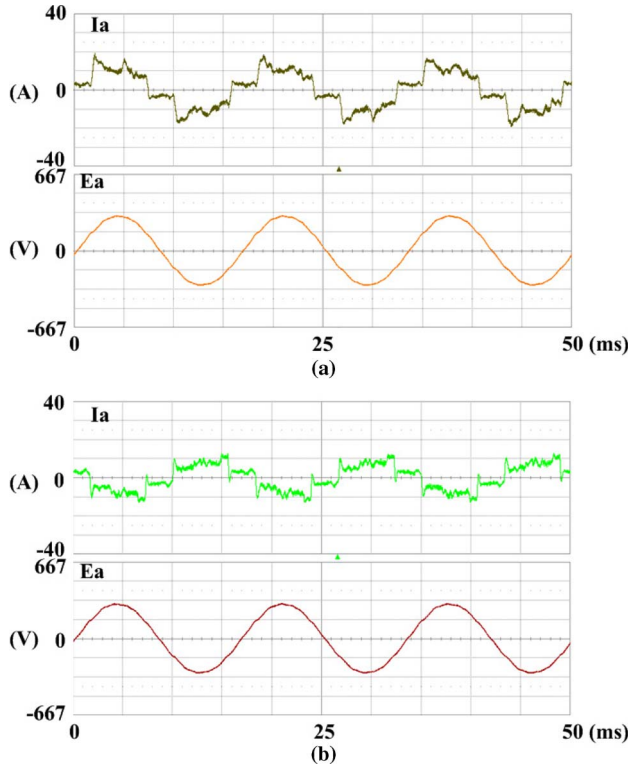

Fig. 4. Input "a" phase current and input "a" phase voltage. (a) Four-kilowatt motoring mode. (b) Three-kilowatt regenerating mode.

loss, the heat sink for the rectifier can be saved remarkably. In addition, the precharging circuit for the dc-link capacitor can be eliminated. A regenerating operation is also possible, owing to the inherent bidirectional power flow capability of the bidirectional rectifier.

Fig. 4(a) and (b) shows the experimental results when the 7.5-kW induction machine driven by the electrolytic-capacitor-less inverter is running in motoring mode and regenerating mode, respectively.

In Fig. 4, "Ia" is the "a" phase input current, and "Ea" is the "a" phase input voltage. Fig. 4 also shows that the displacement power factor is nearly one regardless of whether it is in the motoring or the regenerating operation mode.

III. Flux-Weakening Operation of an Induction Machine With an Electrolytic-Capacitor-Less Inverter

The voltage equation of the induction machine in the synchronous reference frame can be deduced as

$$v_{ds}^e = R_s i_{ds}^e + \sigma L_s \frac{di_{ds}^e}{dt} + \frac{L_m}{L_r}\frac{d\lambda_{dr}^e}{dt} - \omega_e \sigma L_s i_{qs}^e \quad (3)$$

$$v_{qs}^e = R_s i_{qs}^e + \sigma L_s \frac{di_{qs}^e}{dt} + \frac{L_m}{L_r}\omega_e \lambda_{dr}^e + \omega_e \sigma L_s i_{ds}^e \quad (4)$$

where v_{ds}^e, v_{qs}^e, i_{ds}^e, and i_{qs}^e denote the d- and q-axis voltages and currents in the synchronously rotating reference frame, R_s is the stator resistance, L_s is the stator self-inductance, L_r is the rotor self-inductance, L_m is the mutual inductance, λ_{dr}^e is the rotor flux in the synchronous reference frame, ω_e is the operating frequency, and σL_s is the stator transient inductance $(\sigma L_s = L_s - (L_m^2/L_r))$.

In the steady state, the flux and the current in the synchronously rotating reference frame can be considered as constant. As the voltage drop by the stator resistance is quite small compared to the other terms in (3) and (4) in the flux-weakening region, the voltage drop of the stator resistance can be neglected in this region. From the aforementioned assumptions, the voltage equation in the synchronously rotating reference frame can be approximated as

$$v_{ds}^e \cong -\omega_e \sigma L_s i_{qs}^e \quad (5)$$

$$v_{qs}^e \cong \frac{L_m}{L_r}\omega_e \lambda_{dr}^e + \omega_e \sigma L_s i_{ds}^e = \omega_e L_s i_{ds}^e. \quad (6)$$

The developed torque in the steady state can be expressed as

$$T_e = \frac{3}{2}\frac{P}{2}\frac{L_m}{L_r}\lambda_{dr}^e i_{qs}^e \quad (7)$$

where T_e is the generated torque and P is the number of poles of the machine.

As the speed increases, the back-electromotive-force value of the induction machine increases, and the flux-weakening operation is thus applied to regulate the torque of the motor. Normally, the developed output torque in the flux-weakening region is limited by both the maximum stator current and the maximum stator voltage. As mentioned in Section II, the voltage margin in the electrolytic-capacitor-less inverter is reduced compared to that of a conventional PWM inverter [14]. Hence, in the case of an electrolytic-capacitor-less inverter, the base speed should also be properly reduced.

In the two limiting conditions, initially, the voltage limit is considered. The maximum stator voltage $V_{s\_\max}$ is determined by the dc-link voltage $V_{\rm dc}$ and the PWM strategy. The voltage limit condition can be simply formulated as

$$(v_{ds}^e)^2 + (v_{qs}^e)^2 \le V_{s\_\max}^2. \quad (8)$$

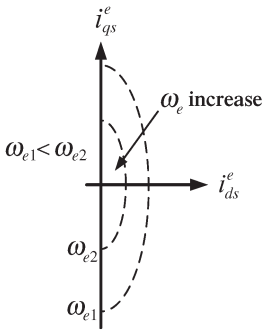

Fig. 5. Voltage limit ellipse in the synchronously rotating reference frame current domain.

From (5), (6), and (8), the voltage limit constraint can be expressed in terms of currents in the synchronously rotating reference frame as

$$\left(\omega_e \sigma L_s i^e_{qs}\right)^2 + \left(\omega_e L_s i^e_{ds}\right)^2 \le V^2_{s\_\max}. \tag{9}$$

This voltage limit boundary is an ellipse, which is a function of the operating frequency ω_e, and the center of the voltage limit ellipse is the origin in the current plane. In the low-speed region, the voltage limit ellipse is large enough; hence, the voltage cannot be a constraint. However, as the operating frequency increases, the voltage limit ellipse shrinks, and the voltage becomes the constraint above a certain speed.

To satisfy the voltage limit constraint in the flux-weakening region, the current trajectory should be inside the voltage ellipse at every operating point, as shown in Fig. 5.

In addition, in the electrolytic-capacitor-less inverter, the maximum allowable stator voltage varies even under the same speed and load torque condition due to the fluctuation of the dc-link voltage, as expressed by (1) and (2). Therefore, to maximize the developed torque, exploiting the fluctuating dc-link voltage in the electrolytic-capacitor-less inverter by as much as possible is preferred.

A second constraint is the current limit. The current boundary is limited by the maximum allowable machine-side inverter current $I_{s\_\max}$. Hence, the current limit can be formulated as

$$(i^e_{ds})^2 + (i^e_{qs})^2 \le I^2_{s\_\max}. \tag{10}$$

As shown in (10), the center of the current limit circle is also the origin in the current plane. The radius of the current limit circle is dependent on the maximum current of the machine-side inverter. To satisfy the current constraint, the currents of the machine should be inside the current limit circle at every operating point.

To satisfy both voltage and current constraints, the current trajectory should be inside the common area of a current limit circle and a voltage limit ellipse. In Fig. 6, the shaded area denotes the available current region according to the dc-link voltage. As shown in the figure, there are two voltage limit ellipses due to the fluctuation of the dc-link voltage. If the voltage limit is too conservatively restricted only by the small ellipse corresponding to $V_{\mathrm{dc}\_\min}$, the developed torque would be small. In contrast, if only large ellipse corresponding to $V_{\mathrm{dc}\_\max}$ is used as a voltage limit, i.e., if an overly radical approach is taken, the current would not be regulated due to a lack of voltage to the machine. Therefore, measuring the dc-link voltage accurately and reflecting the voltage fluctuation in the flux-weakening operation in real time are necessary.

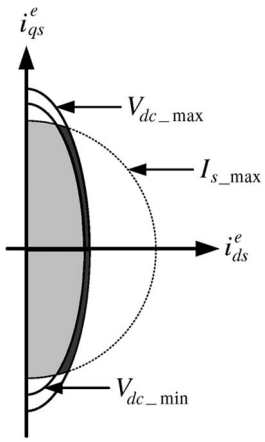

Fig. 6. Voltage limit ellipse and current limit circle of the electrolytic-capacitor-less inverter in the synchronously rotating reference frame current domain.

IV. Proposed Flux-Weakening Strategy

There are several strategies for the flux-weakening operation of an induction machine driven by a PWM inverter [12]. In this paper, the current references are modified as realizable references to maximize the available voltage to the machine.

To regulate the currents in the flux-weakening region, the output voltages of the current regulator should be equal to the demanded stator voltages of the induction machine, which are given by (5) and (6). If the current is not regulated properly due to shortage in the voltage margin in the flux-weakening region, the current references should be modified. Hence, modifying the current references to maximize the voltage utilization in the flux-weakening operation is a major issue. Moreover, the flux-weakening controller and the antiwindup algorithm conflict, as discussed in [15]. Eliminating the antiwindup algorithm in the flux-weakening operation is also recommended. Therefore, the proposed flux-weakening strategy only utilizes the flux-weakening controller without any antiwindup function.

In this paper, the cost function is set to maximize voltage utilization and to reduce the d-axis current reference in the synchronous reference frame appropriately. With the reduced d-axis current reference, the rotor flux in the synchronously rotating reference frame λ^e_{dr} can be controlled for the flux-weakening operation, and the current regulation performance can be maintained. The proposed cost function to maximize the voltage utilization can be set as

$$J = \frac{1}{2}\left((\Delta v^e_{ds})^2 + (\Delta v^e_{qs})^2\right). \tag{11}$$

The voltage differences Δv^e_{ds} and Δv^e_{qs} are defined as

$$\Delta v^e_{ds} = -\omega_e \sigma L_s i^e_{qs} - v_{d,\lim} \tag{12}$$

$$\Delta v^e_{qs} = \omega_e L_s i^e_{ds} - v_{q,\lim} \tag{13}$$

where $v_{d,\lim}$ and $v_{q,\lim}$ are the d- and q-axis maximum realizable voltages in the synchronous reference frame, respectively.

In this paper, minimum error overmodulation is used [12]. Hence, the voltage differences can be calculated easily. Although the maximum realizable voltage of the electrolytic-capacitor-less inverter is fluctuating due to the small dc-link capacitance, it can be considered as a constant value during a sampling period because the sampling frequency of the current regulation loop is much higher than the line voltage frequency. In the constant-torque region, if the voltage margin is sufficient, the voltage differences are usually zero. However, in the flux-weakening region, overmodulation usually occurs due to the increase in the demanded machine voltage. Therefore, a voltage difference arises at each operation point of the flux-weakening region, and the current reference should be modified at the operating point to resolve the difference.

The amount of the modified d-axis current reference which minimizes the voltage difference of (11) can be calculated by (14) using gradient-descent method [15]

$$\begin{aligned}\begin{bmatrix} \frac{di_{ds}^e}{dt} \\ \frac{di_{qs}^e}{dt} \end{bmatrix} &= -\begin{bmatrix} \alpha_1 & 0 \\ 0 & \alpha_2 \end{bmatrix} \Delta J \\ &= -\begin{bmatrix} \alpha_1 & 0 \\ 0 & \alpha_2 \end{bmatrix} \begin{bmatrix} \frac{\partial J}{\partial i_{ds}^e} \\ \frac{\partial J}{\partial i_{qs}^e} \end{bmatrix} \\ &= -\begin{bmatrix} \alpha_1 & 0 \\ 0 & \alpha_2 \end{bmatrix} \begin{bmatrix} 0 & \omega_e L_s \\ -\omega_e \sigma L_s & 0 \end{bmatrix} \begin{bmatrix} \Delta v_{ds}^e \\ \Delta v_{qs}^e \end{bmatrix}. \end{aligned} \quad (14)$$

In (14), α_1 and α_2 are the gains which determine the performance of the flux-weakening operation. A larger gain implies poorer voltage utilization. To increase the voltage utilization, it is better to set a small gain. However, a smaller gain leads to larger current ripples due to a lack of a voltage margin in the current regulation. By integrating (14), the amount of current modification can be obtained. However, to circumvent the offset problem, which may result in divergence of the amount of the current modification term, a high-pass-filtered voltage difference, whose cutoff frequency is around several hertz, can be used instead of (12) and (13), and then, the offset voltage can be removed. By integrating the high-pass-filtered voltage difference, the amount of current modification can be obtained. Hence, the amount of current reference modification can be deduced by

$$\begin{bmatrix} \Delta i_{ds}^e \\ \Delta i_{qs}^e \end{bmatrix} = -\begin{bmatrix} \frac{\alpha_1}{s} & 0 \\ 0 & \frac{\alpha_2}{s} \end{bmatrix} \begin{bmatrix} \frac{s}{s+\omega_1} & 0 \\ 0 & \frac{s}{s+\omega_2} \end{bmatrix} \begin{bmatrix} \omega_e L_s \Delta v_{qs}^e \\ -\omega_e \sigma L_s \Delta v_{ds}^e \end{bmatrix}. \quad (15)$$

Finally, the modified current references in the flux-weakening region can be described as

$$i_{ds,m}^e = i_{ds}^{e^*} + \frac{1}{s+\omega_1}\left(-\alpha_1 \omega_e L_s \Delta v_{qs}^e\right) \quad (16)$$

$$i_{qs,m}^e = i_{qs}^{e^*} + \frac{1}{s+\omega_1}\left(\alpha_2 \omega_e \sigma L_s \Delta v_{ds}^e\right) \quad (17)$$

where $i_{ds,m}^e$ and $i_{qs,m}^e$ are the modified d- and q-axis current references in the flux-weakening region, respectively, and $i_{ds}^{e^*}$ and $i_{qs}^{e^*}$ are the d- and q-axis current references in the constant-torque region, respectively.

The magnitudes of the modification part of the current reference increase as the voltage differences increase, which indicates a deeper flux-weakening operation.

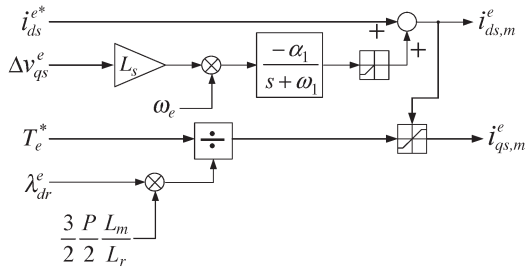

Fig. 7. Block diagram of the proposed current reference generation scheme in the flux-weakening region.

As shown in (15), the proposed flux-weakening operation is based on an integral controller. If the proportional–integral (PI) controller is used instead of the integral controller, the current modification is based on the bandpass-filtered voltage difference, and the modification process may be complex. In the same way, if only the proportional controller is used, the current modification would be dependent on the high-pass-filtered voltage difference directly, and the oscillation of the current reference would be severe compared to that of the proposed method.

There are several types of flux-weakening strategies for the induction machine based on the square or magnitude of the voltage difference [17]. However, considering the steady state and ignoring the voltage drop by the stator resistance, the only q-axis voltage difference is related to the d-axis current modification as shown in (16).

From (13) and (16), it seems that the d-axis current reference of the proposed flux-weakening strategy decreases with the square of the operating frequency. However, the amount of d-axis current modification is influenced by the production of L_s and α_1. If the gain α_1 is small, the amount of modification of the d-axis current of the proposed method is not larger than that of the conventional "ω_r" method which linearly decreases the d-axis current reference according to the rotor speed.

From (16), the d-axis current reference can be obtained for the flux-weakening operation. However, the developed torque, which is shown in (7), cannot be maintained. In order to maintain the torque, the q-axis current reference of (17) should be replaced with (18) if there is a margin in the available maximum current

$$i_{qs,m}^e = \frac{T_e^*}{\frac{3}{2}\frac{P}{2}\frac{L_m}{L_r}\lambda_{dr}^e} \quad (18)$$

where T_e^* is the torque reference.

In (18), the rotor flux λ_{dr}^e can be obtained using a closed-loop Gophinath flux observer, which is presented as (19) deduced in [16]

$$\lambda_{dr}^e = \frac{L_m}{\frac{L_r}{R_r}s+1} i_{ds}^e. \quad (19)$$

In addition, to satisfy the current limit condition, the q-axis current reference of (18) should be modified as

$$i_{qs,m}^e = \min\left(\frac{T_e^*}{\frac{3}{2}\frac{P}{2}\frac{L_m}{L_r}\lambda_{dr}^e}, \sqrt{I_{s\_\max}^2 - (i_{ds,m}^e)^2}\right). \quad (20)$$

Fig. 7 shows a block diagram of the proposed current reference generation in the flux-weakening region. In Fig. 7, there

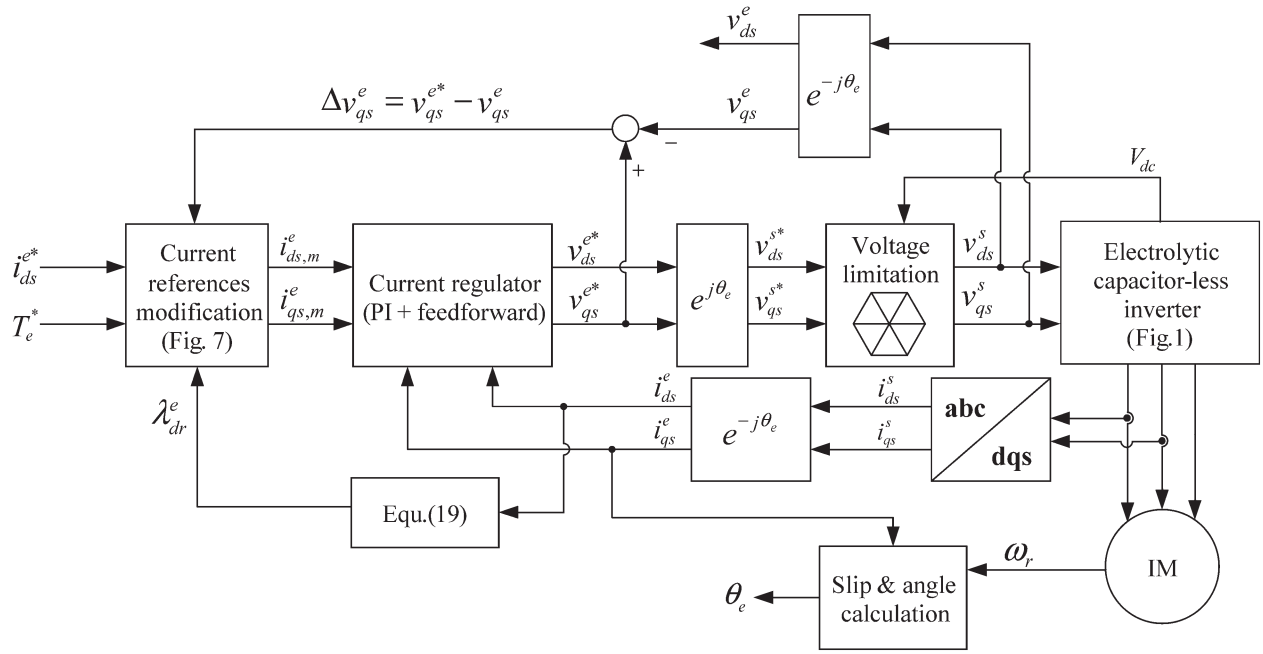

Fig. 8. Block diagram of the proposed flux-weakening operation.

TABLE I
NOMINAL PARAMETERS OF A MOTOR UNDER TEST

Quantity	Value [Unit]
Rs	0.568[Ω]
σLs	8.04[mH]
Lm	88.6[mH]
Rr	0.374[Ω]
Pole pair	2
Rated power	7.5[kW]
Rated voltage	380[V_{rms}]
Rated current	19.2[A]
Rated speed	1730[r/min]

TABLE II
PARAMETERS OF THE ELECTROLYTIC-CAPACITOR-LESS INVERTER

Quantity	Value [Unit]
Input Filter Inductance, L_f	200[μH]
Input Filter Capacitance, C_f (delta-connected)	9[μF] each
Input Filter Resistance, R_f	2.5[Ω]
DC-Link Capacitance, C_{dc}	9[μF]

are two limiters. In the case of an induction machine, the d-axis current reference in the synchronously rotating reference frame should be positive to produce the rotor flux. Hence, a lower limiter is needed to avoid a situation in which the d-axis current is below zero. An upper limiter is necessary to maintain the maximum current rating according to the modified d-axis current reference.

In Fig. 8, a block diagram of the proposed flux-weakening controller, including the inverter and the induction machine, is shown. The current regulator is a synchronously rotating reference frame PI regulator with a feed-forward scheme, and the induction machine is controlled by the indirect field orientation principle. The voltage limit hexagon is determined by the dc-link voltage of the electrolytic-capacitor-less inverter. The voltage difference can be obtained by the overmodulated voltage reference and the output voltage of the current regulator.

V. SIMULATION AND EXPERIMENTAL RESULTS

Table I illustrates the parameters of an induction machine under test, and Table II demonstrates those of the electrolytic-capacitor-less inverter. In this paper, an LC filter with a damping resistor is used as the input filter, where L_f is the inductance, C_f is the capacitance, and R_f is the parallel resistance of the input filter. As shown, the capacitance in the dc link $C_{\rm dc}$ is only 9 μF, and the total capacitance is only 22.5 μF, which is less than 0.5% of that of the conventional PWM VSI with a similar power rating. Fig. 9 shows the photographs of a prototype electrolytic-capacitor-less inverter and the control circuit used for the experimental test.

To determine the level of performance of the proposed flux-weakening strategy, the induction machine under test is operated in torque control mode, and the load machine, which is directly coupled to the test machine, is operated in speed control mode.

Fig. 10 shows the simulation result of the proposed flux-weakening operation when the induction machine is accelerated from 0 to 2000 r/min during 1 s under rated load. As shown, the current is well regulated, and the voltage difference determines the magnitude of the current modification.

Fig. 11 shows the experimental result when the induction machine is running at 2000 r/min under rated load, where the induction machine operated in the flux-weakening region. In Fig. 11, "Ia" is the "a" phase input current, and "Vdc" is the dc-link voltage.

As shown in the figure, the dc-link voltage is fluctuating at six times the input frequency, and the "a" phase input current is a quasi-square wave.

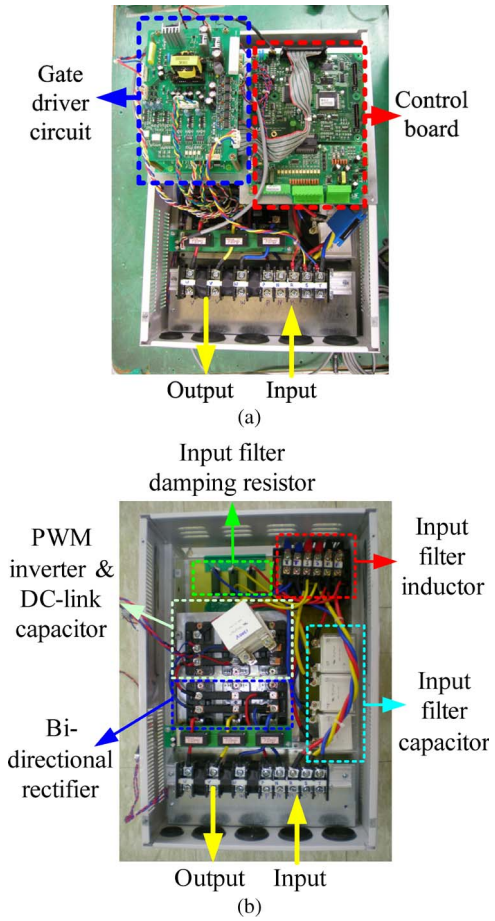

Fig. 9. Prototype electrolytic-capacitor-less inverter. (a) Control circuit. (b) Power stack.

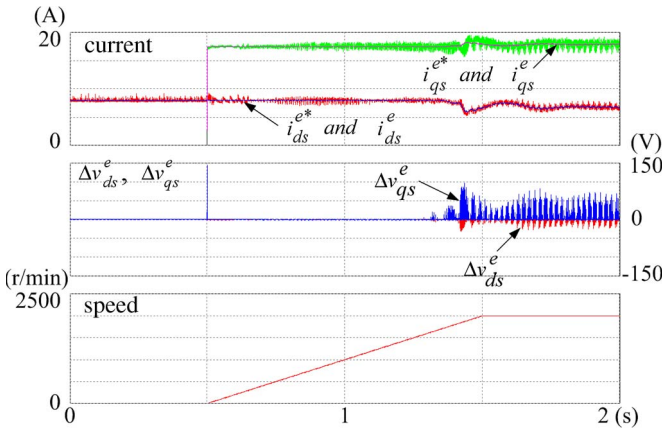

Fig. 10. Simulation result of the proposed flux-weakening strategy.

Fig. 12 shows the current regulation performance of the proposed flux-weakening strategy. In Fig. 12, i_{ds}^{e}, i_{qs}^{e}, and ω_{rpm} are the d- and q-axis currents in the synchronously rotating reference frame and the mechanical rotor speed, respectively. In Fig. 12(a), the induction machine is operated in motoring mode, accelerating from 1500 to 2000 r/min under full load when the gain α_1 is set to -0.03. As shown in the figure, the d-axis current decreases to reduce the rotor flux, while the q-axis current increases to maximize the developed torque when the rotor speed increases. In Fig. 12(b), the induction machine

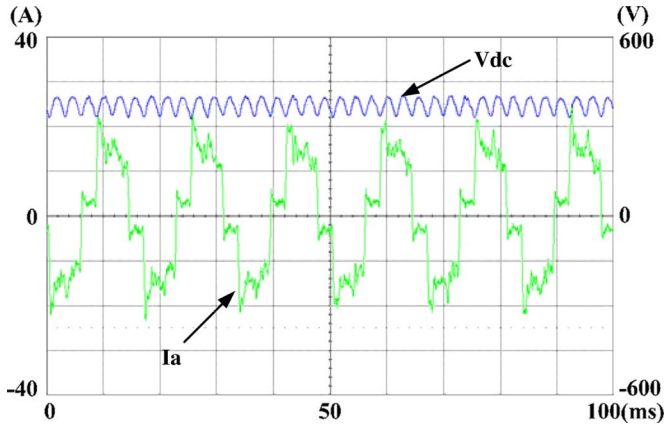

Fig. 11. Input current and sampled dc-link voltage at 2000 r/min.

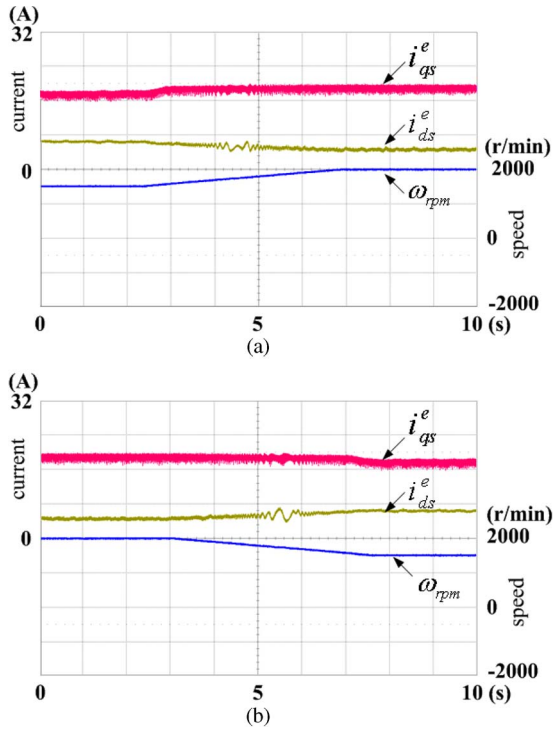

Fig. 12. Currents of the proposed flux weakening in motoring mode. (a) From 1500 to 2000 r/min. (b) From 2000 to 1500 r/min.

is decelerated from 2000 to 1500 r/min. As the operating point of the induction machine varies, the currents are modified to maximize the voltage utilization.

Fig. 13 shows the current regulation performance in the regenerating mode. In Fig. 13, the gain is -0.03, and the induction machine is accelerated under full load from -1500 to -2000 r/min and decelerated from -2000 to -1500 r/min. Modification of the current is suitably performed without an unstable point.

In Figs. 12 and 13, although there is some oscillation in the d-axis current, the modified q-axis current has less oscillation considering the rotor time constant. From Figs. 12 and 13, it can be concluded that the proposed flux-weakening strategy is acceptable under a fluctuating dc-link voltage.

Fig. 14 shows the current trajectory in the synchronously rotating d–q current plane. The red dotted circle is the current

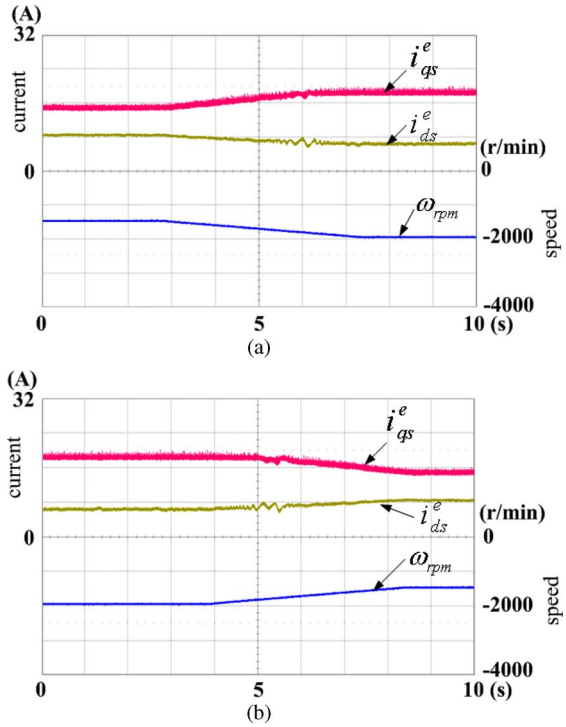

Fig. 13. Currents of the proposed flux weakening in regenerating mode. (a) From −1500 to −2000 r/min. (b) From −2000 to −1500 r/min.

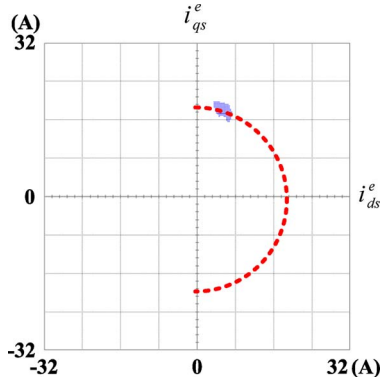

Fig. 14. Current trajectory of the proposed flux weakening in the synchronous reference frame current domain.

limit circle. As shown, the currents are on the current limit circle to maximize the developed torque.

Fig. 15 also shows the d- and q-axis voltage trajectories in the stationary reference frame. In Fig. 15, v^s_{ds} and v^s_{qs} are the d- and q-axis voltages in the stationary reference frame, respectively. The red solid line is the voltage limit hexagon considering the maximum value of the dc-link voltage; the red dotted line is that considering the minimum dc-link voltage. The blue dots, which appear as a cloud, are the actual voltage references at each sampling instant when the induction machine is operated at 2000 r/min. In Fig. 15(a), the gain α_1 is set as -0.03, and in Fig. 15(b), it is set as -0.003. When the gain is smaller, more voltage can be used.

However, it is unavoidable that a larger current ripple arises when the gain is smaller. Even when a relatively small voltage is used with a large gain, the magnitude of the synthesized voltage is larger than the hexagon of the minimum dc-link

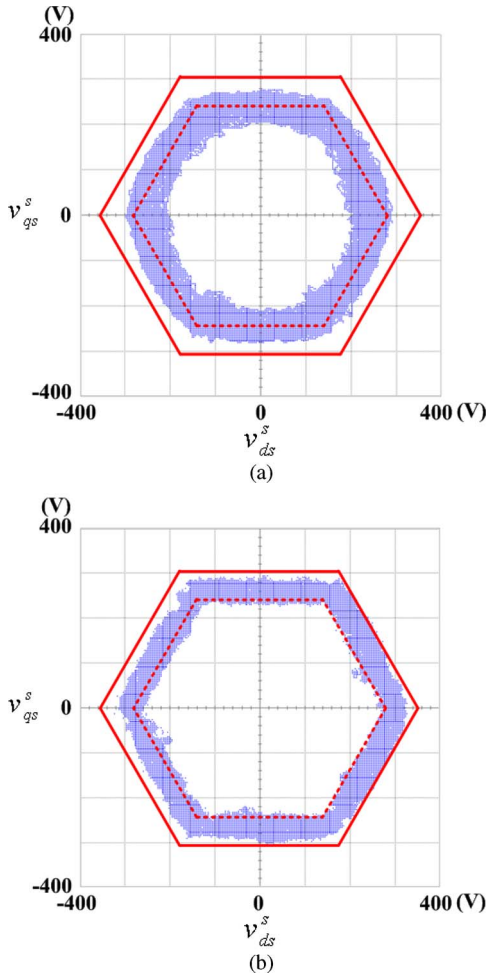

Fig. 15. Voltage trajectory in the stationary voltage reference frame at 2000 r/min. (a) Proportional gain is set as −0.03. (b) Proportional gain is set as −0.003.

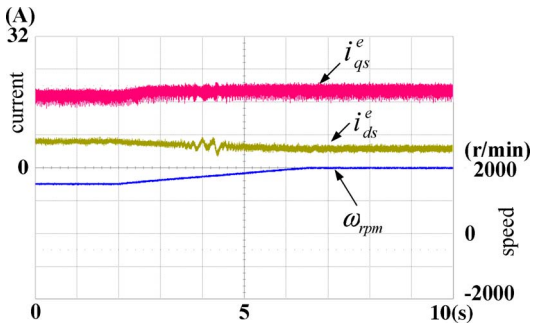

Fig. 16. Current and rotor speed of the proposed flux weakening at motoring mode when the gain is set to −0.003.

voltage. Fig. 15 shows that the proposed flux-weakening strategy exploits the dc-link voltage maximally regardless of the continuous fluctuation of the dc-link voltage. However, the available voltage to the machine varies according to the gain. Nonetheless, the voltage remains above the hexagon set by $V_{\mathrm{dc\_min}}$.

Fig. 16 shows the current and the rotor speed when the gain is set as −0.003. As shown, when the gain is smaller, the current ripple is richer.

VI. Conclusion

In the case of an electrolytic-capacitor-less inverter, there is no reactive component in the dc link apart from film capacitors of several microfarads that are used for snubbering purposes. Due to its small capacitance, the THD value of the input currents is improved remarkably compared to that of the conventional PWM VSI. However, the dc-link voltage is fluctuating, and it is difficult to operate the induction machine properly in the flux-weakening region.

In this paper, a novel flux-weakening strategy for an induction machine driven by an electrolytic-capacitor-less inverter has been proposed to maximize the voltage to the induction machine in the flux-weakening region. The proposed flux-weakening strategy modifies the current references to exploit the dc-link voltage maximally. The experimental results verified the feasibility and superiority of the proposed strategy. Although the available voltage to the machine varies according to the gain, the voltage remains above the hexagon set by $V_{\mathrm{dc\_min}}$.

References

[1] Military Handbook 217 F, "Reliability prediction of electronic equipment," Revision F, Dec. 1991, Notice 1, Jul. 1992, Notice 2, Feb. 1995.

[2] S. Kim, S. K. Sul, and T. A. Lipo, "AC/AC power conversion based on matrix converter topology with unidirectional switches," *IEEE Trans. Ind. Appl.*, vol. 36, no. 1, pp. 139–145, Jan./Feb. 2000.

[3] M. Hinkkanen and J. Luomi, "Induction motor drives equipped with diode rectifier and small DC-link capacitance," *IEEE Trans. Ind. Electron.*, vol. 55, no. 1, pp. 312–320, Jan. 2008.

[4] M. Alakula and J. E. Persson, "Vector controlled AC/AC converters with a minimum of energy storage," in *Conf. Rec. IEEE IAS Annu. Meeting*, Oct. 1994, vol. 2, pp. 1130–1134.

[5] L. Malesani, L. Rossetto, P. Tenti, and P. Tomasin, "AC/DC/AC PWM converter with reduced energy storage in the DC link," *IEEE Trans. Ind. Appl.*, vol. 31, no. 2, pp. 287–292, Mar./Apr. 1995.

[6] J. S. Kim and S. K. Sul, "New control scheme for AC–DC–AC converter without DC link electrolytic capacitor," in *Conf. Rec. IEEE PESC*, Jun. 1993, pp. 300–306.

[7] M. Hinkkanen, L. Harnefors, and J. Luomi, "Control of induction motor drives equipped with small DC-link capacitance," in *Conf. Rec. IEE-EPE*, Sep. 2007, pp. 1–10.

[8] S. H. Kim and S. K. Sul, "Maximum torque control of an induction machine in the field weakening region," *IEEE Trans. Ind. Appl.*, vol. 31, no. 4, pp. 787–794, Jul./Aug. 1995.

[9] X. Xu and D. W. Novotny, "Selection of the flux reference for induction machine drives in the field weakening region," *IEEE Trans. Ind. Appl.*, vol. 28, no. 6, pp. 1353–1358, Nov./Dec. 1992.

[10] S. H. Kim and S. K. Sul, "Voltage control strategy for maximum torque operation of an induction machine in the field-weakening region," *IEEE Trans. Ind. Electron.*, vol. 44, no. 4, pp. 512–518, Aug. 1997.

[11] G. G. Lopez, F. S. Gunawan, and J. E. Walters, "Current control of induction machine in the field-weakened region," *IEEE Trans. Ind. Appl.*, vol. 43, no. 4, pp. 981–989, Jul./Aug. 2007.

[12] F. Briz, A. Diez, M. W. Degner, and R. D. Lorenz, "Current and flux regulation in field-weakening operation," *IEEE Trans. Ind. Appl.*, vol. 37, no. 1, pp. 42–50, Jan./Feb. 2001.

[13] A. Yoo, W. J. Lee, S. Kim, B. M. Dehkordi, and S. K. Sul, "Input filter analysis and resonance suppression control for electrolytic capacitor-less inverter," in *Conf. Rec. IEEE APEC*, Feb. 2008, pp. 1786–1792.

[14] B. Piepenbreier and L. Sack, "Regenerative drive converter with line-frequency switched rectifier and without DC link components," in *Conf. Rec. IEEE PESC*, 2004, pp. 3917–3923.

[15] T. S. Kwon, G. Y. Choi, M. S. Kwak, and S. K. Sul, "Novel flux-weakening control of an IPMSM for quasi six-step operation," *IEEE Trans. Ind. Appl.*, vol. 44, no. 6, pp. 1722–1731, Nov./Dec. 2008.

[16] P. L. Jansen and R. D. Lorenz, "A physically insightful approach to the design and accuracy assessment of flux observers for field oriented induction machine drives," *IEEE Trans. Ind. Appl.*, vol. 30, no. 1, pp. 101–110, Jan./Feb. 1994.

[17] L. Harnefors, K. Pietilainen, and L. Gertmar, "Torque-maximizing field-weakening control: Design, analysis, and parameter selection," *IEEE Trans. Ind. Electron.*, vol. 48, no. 1, pp. 161–168, Feb. 2001.

Anno Yoo (S'07–M'10) was born in Seoul, Korea, in 1977. He received the B.S., M.S., and Ph.D. degrees in electrical engineering from Seoul National University, Seoul, in 2004, 2006, and 2010, respectively.

Since 2010, he has been a Senior Researcher with the Central R&D Center, LSIS, Anyang, Korea. His current interests include high-performance ac drive systems, high-power converter design, and electric/hybrid vehicle drives.

Seung-Ki Sul (S'78–M'80–SM'98–F'00) was born in Korea in 1958. He received the B.S., M.S., and Ph.D. degrees in electrical engineering from Seoul National University, Seoul, Korea, in 1980, 1983, and 1986, respectively.

From 1986 to 1988, he was an Associate Researcher in the Department of Electrical and Computer Engineering, University of Wisconsin, Madison. From 1988 to 1990, he was a Principal Research Engineer with Goldstar Industrial Systems Company. Since 1991, he has been a Member of the Faculty of the School of Electrical Engineering, Seoul National University, where he is currently a Professor. His current research interests include the power electronic control of electric machines, electric/hybrid vehicle drives, and power converter circuits.

Hyeseung Kim was born in Korea in 1979. She received the B.S. and M.S. degrees in electrical engineering from Konkuk University, Seoul, Korea, in 2003 and 2005, respectively.

She is currently with the Central R&D Center, LSIS, Anyang, Korea. Her research interests include ac machine drives and elevator systems.

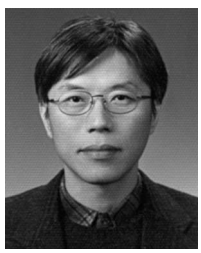

Kyung-Seo Kim (S'88–M'90) received the B.S., M.S., and Ph.D. degrees in electrical engineering from Seoul National University, Seoul, Korea, in 1982, 1984, and 1990, respectively.

Since 1984, he has been with LSIS, Anyang, Korea, where he is currently a Research Fellow in the Central R&D Center. From 1991 to 1992, he was a Postdoctoral Fellow at The University of Tennessee, Knoxville. His research interests are in the areas of electric vehicle drives, power converters for renewable energy, and smart grids.